

A Supervisory Frequency Support Control Scheme for Distributed PV

Qinmiao Li, *Student Member, IEEE*, Mesut Baran, *Fellow, IEEE*

Abstract—Increasing penetration of Photovoltaic (PV) generation brings an opportunity, and sometimes necessity, for this new resource to provide ancillary services such as frequency support. Recent efforts toward this goal focused mainly on the large-scale PV plants, and the proposed methods may not be easily adopted for distributed PV, which are smaller in size and connected to distributed systems. In this paper, we propose a novel control scheme for the same purpose but focusing on distributed PV. To address the diversities among distributed PV, we first derive a reduced-order aggregate model to represent their overall dynamic behavior. Then, using this model, a tracking linear quadratic regulator (LQR) based controller is used as a supervisory controller that can control a group of distributed PV to provide frequency support. We also propose an inversion method for the controller to invert the control signals for aggregate model back to each individual PV's. The proposed reduced-order aggregate model is validated against a group of distributed PV systems represented by detailed nonlinear models. We also demonstrate the effectiveness of the control scheme, as well as the inversion method, through time-domain simulations using a standard test system.

Index Terms—Aggregate model, Distributed PV, Frequency response, Linear quadratic regulator (LQR), Small-signal model

I. INTRODUCTION

PHOTOVOLTAIC (PV) generation has been fast growing in recent years [1], [2]. A considerable portion of the increasing PV installation are the small-size distributed PV in distribution systems which are projected to continue growing [3], [4]. PV systems are inverter-based systems without rotating inertia and governor systems. Therefore, they do not have any frequency support capability, and their high penetration poses negative impacts on the bulk system frequency response such as low frequency nadir, large rate of change of frequency (RoCoF) [5]–[7]. Recently, several grid codes or orders from system operators and regulatory authorities started requiring commercial PV plants to provide frequency support during disturbances [8]–[11]. Meanwhile, leveraging distributed PV for grid services has also become imperative, especially for small-scale power systems with high penetration of distributed PV. For example, the Hawaiian Electric is seeking frequency support from aggregators of distributed rooftop PV [12].

Methods for enabling frequency support from PV systems can be found in the literature. One approach is referred to as de-loading control [13], in which the PV's operating point is first set below its maximum power point (MPP). Then the PV array's voltage is controlled to adjust the output power in response of frequency changes. Following this idea, authors in [14], [15] proposed frequency-droop controllers by using Newton quadratic interpolation and a lookup-table (LUT) based approach, respectively. Another method for providing

frequency support from PV systems is to utilize the energy stored in DC-link capacitors and this can be achieved by adjusting the DC-link voltage, as presented in [16], to emulate inertial power response. Reference [17] and [18] also investigate the potential of combining the above two methods.

The aforementioned methods usually consider one single PV system or the large-scale PV plant that consists of identical subsystems. In this paper, however, we focus on the use of small-scale distributed PV (such as rooftop PV) to provide similar frequency support function. Since in practical, distributed PV systems are easier to be managed by aggregators (at community or distribution level), we consider the control scheme for a large group of distributed PV. The goal is to first aggregate the small PV together to act like a large-scale PV plant and then design control scheme to provide effective frequency support. In addition, aggregating distributed PV for control purpose can also simplify the control design and reduce the communication requirements. Following this approach, a fuzzy controller is proposed in [19] to regulate system frequency using distributed PV. However, the PV system model is simplified by neglecting control dynamics and only the insulation difference is considered among the PV systems.

The main challenge in aggregating a group of distributed PV, which are mainly single-phase, is the variation in their capacities, control parameters and working conditions. In this paper, we first propose a new reduced-order aggregate model to represent the overall dynamic behavior of such a group of distributed PV by considering the variations among individual PV. Then, using this model, we adopt a frequency-tracking controller [18] to provide supervisory frequency support from these distributed PV. This controller contains an unknown input observer (UIO) based tracking linear quadratic regulator (LQR) and an LUT. The main motivation of choosing this method is that it can assure the overall system frequency response to be as desired. In this proposed control scheme, which is illustrated in Fig. 1, we also propose an effective inversion method to invert the aggregate control signal to individual ones for each PV system.

In the literature, however, there is limited work on aggregate models for PV systems. An aggregate model for distributed PV with synchronous power controllers is proposed in [20]. However, the electrical part of PV system is modeled as just a current source with a first-order filter. Considering full components, study in [21] derives an aggregate model but only for multiple identical PV systems. For the case with different parameters, order reduction techniques are only suggested but no further details or examples are provided. In this paper, we derive a reduced-order aggregate model which addresses the above shortcomings. The obtained aggregate model is very similar to the small-signal model (SSM) for one PV system and

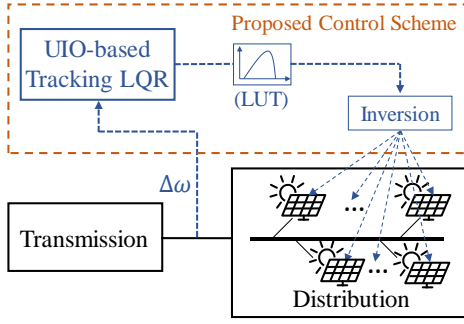


Fig. 2. Conceptual diagram of proposed control scheme.

with the same order. Thus, the advantages are that, 1) model variables still have physical meanings which greatly facilitate control design and its implementation to a real system; 2) computation effort is reduced by retaining the same order as one PV system model.

Hence, the contributions of this paper are: i) A reduced-order aggregate model that can represent the dynamics of a diverse group of distributed PV; ii) An aggregate-model-based control scheme for distributed PV to provide frequency support to the grid. Section II of the paper introduces the new aggregate model. The proposed controller and test results are presented in Section III and IV. Conclusions are included in section V.

II. THE REDUCED-ORDER AGGREGATE MODEL FOR DISTRIBUTED PV

In this section, we first introduce the SSM for one single-phase PV system. Then we derive its aggregate version for a group of distributed PV with different power ratings, control parameters, and solar irradiation.

A. The Single-phase PV System

For one of the single-phase distributed PV, we consider it as a two-stage PV system, which is illustrated in Fig. 2. For such a PV system, existing models are liable to different limitations when they are considered for designing supervisory frequency support controller. For example, some models make simplifications by ignoring PV array characteristics and DC-link dynamics [22]-[24]. Another limitation is the lack of supervisory control input in the models, without which the output power cannot be adjusted in response of frequency [25]-[27]. The SSM proposed in [18] successfully avoids above shortcomings. However, it is derived for three-phase PV systems.

For the electrical part in Fig. 2, we assume the PV array consists of N_{PV} identical PV panels connected in parallel. Its terminal voltage V_{PV} is raised by a boost converter. The DC-link serving as the energy buffer is in between of the converter and a single-phase inverter. An $R-L$ filter is used to interface with the grid. For the local control of this PV system, the rapid active power control (RAPC) method [15] is used at boost converter to determine the operating point of PV array and thus adjust the PV power output. A revised dual-loop current mode controller with feedforward compensation [25] is adopted for inverter control, as shown in Fig. 3. ΔV_{PV} and ΔV_{dc}^{ref} are the two control input that we added to the above local controllers for designing supervisory frequency support control functions.

Compared to the three-phase PV system in [18], the single-

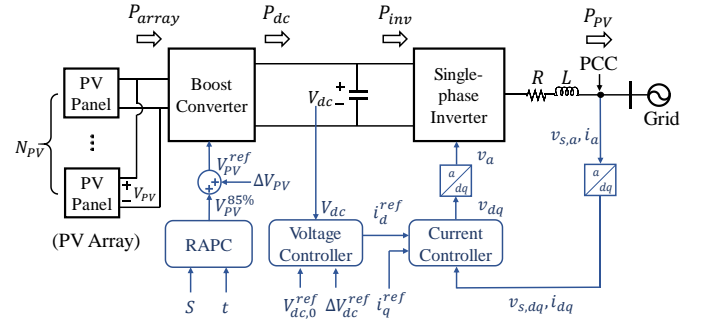


Fig. 3. Diagram for one single-phase two-stage PV system.

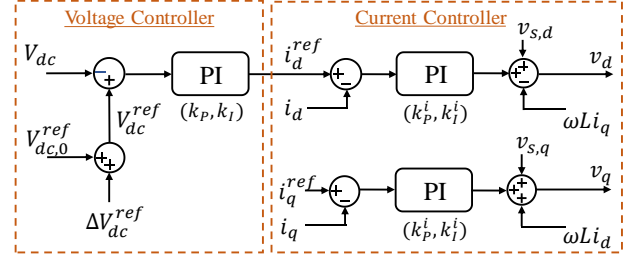


Fig. 1. Diagram of the dual-loop current mode controller.

phase PV system shares the same topology and local control scheme. The only difference that we need to address is the power balance equation:

$$P_{PV} = \frac{1}{2}(i_d v_{sd} + i_q v_{sq}) = \frac{1}{2} i_d v_{sd} \quad (1)$$

in which i_d , i_q and v_{sd} , v_{sq} are the dq components of current and voltage at point of common coupling (PCC), respectively. They can be obtained by the single-phase dq transformation based on the system voltage ($v_{s,a}$) [28]. The ω and θ used in the transformation are provided by an ideal phase-locked loop (PLL). The PLL also regulates v_{sq} to zero, and thus the simplification in (1) can be made.

Then, we can follow the similar derivation as in [18] for three-phase case to model the rest of the system and obtain the SSM for the single-phase two-stage PV system in Fig. 2:

$$\frac{d\Delta V_{dc}}{dt} = \frac{1}{CV_{dc,0}^{ref}} \left(\frac{N_{PV} g(\Delta V_{PV}, S, t)}{\Delta P_{array}} - \frac{1}{2} \frac{\Delta i_d V_{sd}}{\Delta P_{PV}} \right) \quad (2)$$

$$\frac{d\Delta P_{PV}}{dt} = -\frac{1}{\tau} \Delta P_{PV} - \frac{k_p V_{sd}}{2\tau} \Delta V_{dc} + \frac{k_p V_{sd}}{2\tau} \Delta V_{dc}^{ref} + \frac{V_{sd}}{2\tau} \Delta x \quad (3)$$

$$\frac{d\Delta x}{dt} = -k_i \Delta V_{dc} + k_i \Delta V_{dc}^{ref} \quad (4)$$

where the function $g(\Delta V_{PV}, S, t)$ maps the change of PV array voltage to the change of PV panel's output power under given conditions. This function is best represented by an LUT, as the original function is highly nonlinear. V_{sd} is the nominal terminal voltage which is assumed to be well-regulated by the grid. k_p and k_i are the parameters in voltage loop controller, and τ is the time constant in current loop controller [25]. Δx represents the small-signal increment of a controller state which we introduced to avoid second-order derivative in the model.

B. The Reduced-order Aggregate Model

Let $\mathcal{P} = \{1, 2, 3, \dots, N\}$ denote the set of distributed PV in an area of distribution system. For one PV system $i \in \mathcal{P}$, we have

its SSM in the form of:

$$\frac{d\Delta V_{dc,i}}{dt} = \frac{\left(\frac{P_{r,i}}{P_{pa,i}} g_i(\Delta V_{PV,i}, S_i, t_i) - \Delta P_{PV,i}\right)}{C_i V_{dc,0,i}^{ref}} \quad (5)$$

$$\frac{d\Delta P_{PV,i}}{dt} = -\frac{1}{\tau_i} \Delta P_{PV,i} - \frac{k_{P,i} V_{sd,i}}{2\tau_i} \Delta V_{dc,i} + \frac{k_{P,i} V_{sd,i}}{2\tau_i} \Delta V_{dc,i}^{ref} + \frac{V_{sd,i}}{2\tau_i} \Delta x_i \quad (6)$$

$$\frac{d\Delta x_i}{dt} = -k_{I,i} \Delta V_{dc,i} + k_{I,i} \Delta V_{dc,i}^{ref} \quad (7)$$

where $P_{r,i}$ and $P_{pa,i}$ are the rated power of the PV system and one PV panel, respectively, and $N_{PV,i}$ is replaced by $P_{r,i}/P_{pa,i}$. Before aggregating the SSMs for all PV systems in \mathcal{P} , we need to make a few assumptions on the model parameters.

a.1) PV Panel: PV panels used in small PV systems usually have similar characteristics. Hence, we can assume that the PV panels are the same for all PV systems in \mathcal{P} , and thus, $\forall i \in \mathcal{P}$:

$$P_{pa,i} = P_{pa} \quad (8)$$

$$g_i(\Delta V_{PV,i}, S_i, t_i) = g(\Delta V_{PV,i}, S_i, t_i) \quad (9)$$

Also, since the PV systems are within the same area of distribution system, the ambient temperature for PV array will not vary a lot, i.e. $\forall i \in \mathcal{P}: t_i = t$. For solar irradiance, however, we keep the variance among each PV system because the cloud distribution can be different within the area.

a.2) System Voltage: Since the voltage in a distribution system is well-regulated, we can neglect the small variations in PV system terminal voltages and assume $\forall i \in \mathcal{P}: V_{sd,i} = V_{sd}$.

a.3) Control Parameters: For the inverter controller which regulates the DC-link voltage, the voltage level mainly depends on the inverter output voltage. Since all the PV systems are in the same distribution system with the same voltage level, we can then assume identical DC-link voltage references for each one, and hence $\forall i \in \mathcal{P}: V_{dc,0,i}^{ref} = V_{dc,0}^{ref}$.

The other control parameter is the current control loop time constant τ_i . This constant has to be very small such that the current loop is sufficiently fast to coordinate with outer voltage loop. Therefore, we can neglect the variations on τ_i and let $\tau_i = \tau$, because the outer voltage loop parameters are more dominant in the controller dynamics.

a.4) DC-link Capacitor: The main principle of choosing the DC-link capacitor value is to stabilize the voltage such that its ripples are within a desired range [24], [29]. Following the design guide in [24], $\forall i \in \mathcal{P}$, we have:

$$C_i = P_{r,i} \times \frac{D^{max} \times T_s^{max}}{\alpha\% \times (V_{dc,0}^{ref})^2} = P_{r,i} \times C_d \quad (10)$$

constant

where D^{max} and T_s^{max} are the maximum values of the boost converter's duty cycle and switching period, respectively, which we assume to be the same for each PV system. The maximum voltage ripple level, $\alpha\%$, is also chosen to be the same. Moreover, if we assume the DC-link voltages to be their nominal value $V_{dc,0}^{ref}$, the capacitance C_i for the i -th PV system

becomes a product of the rated power, $P_{r,i}$, and a constant unit capacitance, C_d , as indicated in (10).

Next, to obtain the aggregate model, we first define some aggregate variables as:

$$P_r^a = \sum_{i \in \mathcal{P}} P_{r,i}, \quad \Delta P_{PV}^a = \sum_{i \in \mathcal{P}} \Delta P_{PV,i}, \quad \Delta x^a = \sum_{i \in \mathcal{P}} \Delta x_i$$

$$\Delta V_{dc}^a = \frac{\sum_{i \in \mathcal{P}} P_{r,i} \Delta V_{dc,i}}{\sum_{i \in \mathcal{P}} P_{r,i}}, \quad \Delta V_{dc}^{ref,a} = \frac{\sum_{i \in \mathcal{P}} P_{r,i} \Delta V_{dc,i}^{ref}}{\sum_{i \in \mathcal{P}} P_{r,i}}$$

$$\Delta V_{PV}^a = \frac{\sum_{i \in \mathcal{P}} P_{r,i} \Delta V_{PV,i}}{\sum_{i \in \mathcal{P}} P_{r,i}}, \quad S^a = \frac{\sum_{i \in \mathcal{P}} P_{r,i} S_i}{\sum_{i \in \mathcal{P}} P_{r,i}}$$

Considering the aforementioned assumptions, these aggregate variables allow us to obtain the following aggregate model by summing up the SSMs in (5)-(7) for all PV systems in \mathcal{P} :

$$\frac{d\Delta V_{dc}^a}{dt} = \frac{1}{C_d V_{dc,0}^{ref} P_{pa}} \underbrace{\frac{\sum_{i \in \mathcal{P}} P_{r,i} g(\Delta V_{PV,i}, S_i, t)}{P_r^a}}_{S.1} - \frac{1}{C_d V_{dc,0}^{ref} P_r^a} \Delta P_{PV}^a \quad (11)$$

$$\frac{d\Delta P_{PV}^a}{dt} = -\frac{1}{\tau} \Delta P_{PV}^a - \frac{V_{sd}}{2\tau} \underbrace{\sum_{i \in \mathcal{P}} k_{P,i} \Delta V_{dc,i}}_{S.2} + \frac{V_{sd}}{2\tau} \underbrace{\sum_{i \in \mathcal{P}} k_{P,i} \Delta V_{dc,i}^{ref}}_{S.3} + \frac{V_{sd}}{2\tau} \Delta x^a \quad (12)$$

$$\frac{d\Delta x^a}{dt} = -\underbrace{\sum_{i \in \mathcal{P}} k_{I,i} \Delta V_{dc,i}}_{S.4} + \underbrace{\sum_{i \in \mathcal{P}} k_{I,i} \Delta V_{dc,i}^{ref}}_{S.5} \quad (13)$$

In (11)-(13), the summation terms (S.1-S.5) indicate that the model order has not been fully reduced. Therefore, we want to represent these summation terms with the aggregate variables in order to further reduce the order. In the following, we will discuss how this is achieved for each term.

b.1) S.1: For this summation term, we approximate it as:

$$\frac{\sum_{i \in \mathcal{P}} P_{r,i} g(\Delta V_{PV,i}, S_i, t)}{P_r^a} \approx g(\Delta V_{PV}^a, S^a, t) \quad (14)$$

The idea of this approximation is to move the weighted averaging on LHS into g on the variables $\Delta V_{PV,i}$ and S_i . Since the function g represents an LUT, it is very difficult to analytically evaluate the error of this approximation. Therefore, we take the numerical approach, which is Monte Carlo simulation (MCS), to assess the error level. For the MCS, we first assume that all the variables ($P_{r,i}$, $\Delta V_{PV,i}$ and S_i) follow normal distributions with certain means and variances. Moreover, we consider the means and variances to be random

TABLE I
VARIABLE DISTRIBUTIONS AND CORRESPONDING PARAMETERS

$P_{r,i}$	$P_{r,i} \sim \mathcal{N}(\mu_P, \sigma_P^2)$	$\mu_P \sim \mathcal{U}(150000, 250000),$ $\sigma_P \sim \mathcal{U}(10, 30)$	
$\Delta V_{PV,i}$	$\Delta V_{PV,i} \sim \mathcal{N}(\mu_V, \sigma_V^2)$	$\mu_V \sim \mathcal{U}(-30, -7.5),$ $\sigma_V \sim \mathcal{U}(2, 7)$	
S_i	$S_i \sim \mathcal{N}(\mu_S, \sigma_S^2)$	$\mu_S \sim \mathcal{U}(40, 70),$ $\sigma_S \sim \mathcal{U}(1, 10)$	

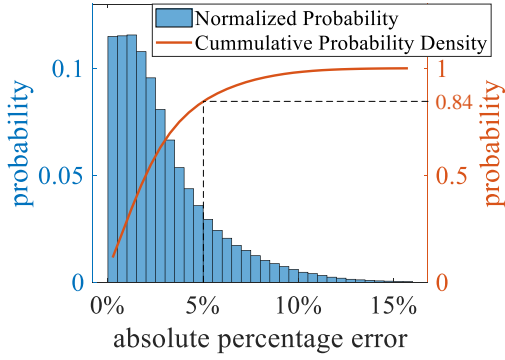


Fig. 4. Probability distribution of the absolute percentage approximation error from MCS

samples from corresponding uniform distributions. Details about the distributions are summarized in TABLE I.

In the MCS, we set the number of trials to be 500,000. In each trial, we sample 50 sets of the three variables and compute the approximation error for (14). Fig. 4 shows the probability distribution of calculated absolute percentage error, as well as the cumulative probability density curve. From the plot, the error is very small for most of the cases, and we have the probability of 84% to get an error below 5%. Therefore, (14) is a good approximation with satisfactory accuracy.

b.2) S.2-S.5: Summation terms S.2-S.5 are discussed together because they share the same structure. Therefore, the same treatment can be applied to all of them. Taking S.2 as an example, we can rearrange it as:

$$\sum_{i \in \mathcal{P}} k_{p,i} \Delta V_{dc,i} = \sum_{i \in \mathcal{P}} \frac{k_{p,i}}{P_{r,i}} P_r^a \Delta V_{dc}^a - \sum_{i \in \mathcal{P}} \left(\sum_{j \in \mathcal{P}, j \neq i} \frac{k_{p,j}}{P_{r,j}} \right) P_{r,i} \Delta V_{dc,i} \quad (15)$$

Note that the summation terms can be further simplified if the following holds:

$$\frac{k_{p,i}}{P_{r,i}} = c_p, \forall i \in \mathcal{P} \quad (16)$$

where c_p is a constant parameter. Equation (16) may not hold in practice, but a good value for c_p can be obtained by minimizing the Euclidean norm of error between $\frac{k_{p,i}}{P_{r,i}}$ and c_p . To achieve this, we may construct an optimization problem to determine c_p as follows:

$$\text{Minimize}_{c_p} \sum_{i \in \mathcal{P}} \left(c_p - \frac{k_{p,i}}{P_{r,i}} \right)^2 \quad (17)$$

Solving the optimization problem, we can obtain:

$$c_p = \frac{\sum_{i \in \mathcal{P}} \left(\frac{k_{p,i}}{P_{r,i}} \right)}{|\mathcal{P}|} \quad (18)$$

where $|\mathcal{P}|$ is the cardinality of set \mathcal{P} . Substitute (16) into (15) to obtain:

$$\sum_{i \in \mathcal{P}} k_{p,i} \Delta V_{dc,i} \approx c_p P_r^a \Delta V_{dc}^a \quad (19)$$

where S.2 is successfully expressed by the aggregate variables.

The same treatment can also be adopted on S.3-S.5 to have:

$$\sum_{i \in \mathcal{P}} k_{p,i} \Delta V_{dc,i}^{ref} \approx c_p P_r^a \Delta V_{dc}^{ref,a} \quad (20)$$

$$\sum_{i \in \mathcal{P}} k_{l,i} \Delta V_{dc,i} \approx c_l P_r^a \Delta V_{dc}^a \quad (21)$$

$$\sum_{i \in \mathcal{P}} k_{l,i} \Delta V_{dc,i}^{ref} \approx c_l P_r^a \Delta V_{dc}^{ref,a} \quad (22)$$

where

$$c_l = \frac{\sum_{i \in \mathcal{P}} \left(\frac{k_{l,i}}{P_{r,i}} \right)}{|\mathcal{P}|} \quad (23)$$

Now we have the reduced-order aggregate model as:

$$\frac{d\Delta V_{dc}^a}{dt} = \frac{1}{C_d V_{dc,0}^{ref}} \left(\frac{g(\Delta V_{PV}^a, S^a, t)}{P_{pa}} - \frac{\Delta P_{PV}^a}{P_r^a} \right) \quad (24)$$

$$\begin{aligned} \frac{d\Delta P_{PV}^a}{dt} = & -\frac{1}{\tau} \Delta P_{PV}^a - \frac{V_{sd}}{2\tau} c_p P_r^a \Delta V_{dc}^a \\ & + \frac{V_{sd}}{2\tau} c_p P_r^a \Delta V_{dc}^{ref,a} + \frac{V_{sd}}{2\tau} \Delta x^a \end{aligned} \quad (25)$$

$$\frac{d\Delta x^a}{dt} = -c_l P_r^a \Delta V_{dc}^a + c_l P_r^a \Delta V_{dc}^{ref,a} \quad (26)$$

Note that this aggregate model is similar to the SSM for one PV system (2)-(4) with the same order. Thus, this model allows us to view the collective dynamics of a group of distributed PV as that of one large-scale PV system, and then design supervisory control for it. Furthermore, the aggregate states and input still correspond to physical quantities, such as ΔP_{PV}^a , which is the total increment power of the distributed PV. This facilitates the later control design, as Section III will show.

III. PROPOSED CONTROL SCHEME

In this section, we introduce the proposed control scheme which contains three main components: a UIO-based tracking LQR, an LUT, and an inversion function, as illustrated in Fig. 1. The tracking LQR is designed to assure that the system frequency can effectively track that of a reference system with given inertia and droop constants (H^{ref} and R^{ref}), under the same unknown disturbance. So that the desired close-loop frequency response capability is achieved with the frequency support from distributed PV. The LUT is introduced to compensate the nonlinearity in the aggregate PV system model and thus obtain a linear plant model for designing the tracking LQR. At last, the inversion function inverts the aggregate control signal, which corresponds to the aggregate model, to individual ones for each distributed PV.

This control scheme is similar to the one in [18] where the large-scale PV plant is focused. However, the differences between our work and [18] are that, 1) a new reduced-order aggregate model is developed and adopted in the tracking LQR for frequency support from distributed PV; 2) an inversion method is developed to obtain the individual control input.

Note that the system/plant for the tracking LQR is the “combined system”, which is the combination of distributed PV, the LUT, and the transmission system. Hence, the model

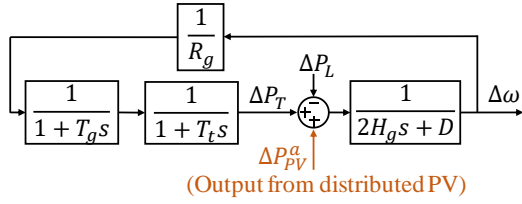


Fig. 5. LFC model including distributed PV

for this combined system is first presented below. Then the components of the tracking LQR are introduced.

A. The Combined System Model

To obtain the combined system model, we first use the classical load frequency control (LFC) model to describe the real power and frequency dynamics in the transmission system. Fig. 5 illustrates the diagram of this model and also how the distributed PV can be tied to this model. From Fig. 5, we can write the LFC model in state-space form as:

$$\begin{cases} \dot{\mathbf{x}}_g = \mathbf{A}_g \mathbf{x}_g + \mathbf{B}_g \mathbf{u}_g + \mathbf{E}_g \mathbf{d}_g \\ \mathbf{y}_g = \mathbf{C}_g \mathbf{x}_g \end{cases} \quad (27)$$

where we treat the increment power ΔP_{PV}^a from distributed PV as an input (\mathbf{u}_g) to the transmission system whereas the load change ΔP_L is taken as the disturbance (\mathbf{d}_g).

Then, for the distributed PV, its derived reduced-order aggregate model in (24)-(26) still contains a nonlinear term which is the LUT function $g(\Delta V_{PV}^a, S^a, t)$. However, the LQR design is facilitated if the plant (combined system) model is linear. Therefore, we add another LUT block between the tracking LQR and distributed PV, as shown in Fig. 1. If this LUT is chosen as the inverse of g :

$$\Delta V_{PV}^a = g^{-1}(\Delta P_{PV}^{ref,a}, S^a, t) \quad (28)$$

The plant seen by the tracking LQR becomes a linear model by substituting (28) into (24). This linear model can be written in the state-space form as:

$$\begin{cases} \dot{\mathbf{x}}_{PV} = \mathbf{A}_{PV} \mathbf{x}_{PV} + \mathbf{B}_{PV} \mathbf{u}_{PV} \\ \mathbf{y}_{PV} = \mathbf{C}_{PV} \mathbf{x}_{PV} \end{cases} \quad (29)$$

where $\mathbf{x}_{PV} = [\Delta V_{dc}^a \ \Delta P_{PV}^a \ \Delta x^a]^T$, $\mathbf{u}_{PV} = [\Delta P_{PV}^{ref,a} \ \Delta V_{dc}^{ref,a}]^T$, and $\mathbf{y}_{PV} = [\Delta P_{PV}^a]$.

Now we can combine the two linear models for both transmission system (27) and distributed PV (with an LUT) (29) through the interfacing variable ΔP_{PV}^a . The obtained model is referred to as the combined system model, which is used as the plant model for the following design of tracking LQR. The combined system model can also be described in state-space as:

$$\begin{bmatrix} \dot{\mathbf{x}}_g \\ \dot{\mathbf{x}}_{PV} \end{bmatrix} = \begin{bmatrix} \mathbf{A}_g & \mathbf{B}_g \mathbf{C}_{PV} \\ 0 & \mathbf{A}_{PV} \end{bmatrix} \begin{bmatrix} \mathbf{x}_g \\ \mathbf{x}_{PV} \end{bmatrix} + \begin{bmatrix} 0 \\ \mathbf{B}_{PV} \end{bmatrix} \mathbf{u}_c + \begin{bmatrix} \mathbf{E}_g \\ 0 \end{bmatrix} \mathbf{d}_c \quad (30)$$

$$\mathbf{y}_c = \mathbf{C}_c \mathbf{x}_c \quad (31)$$

where the output \mathbf{y}_c is frequency deviation $\Delta\omega$. Details of the matrices are provided in Appendix A.

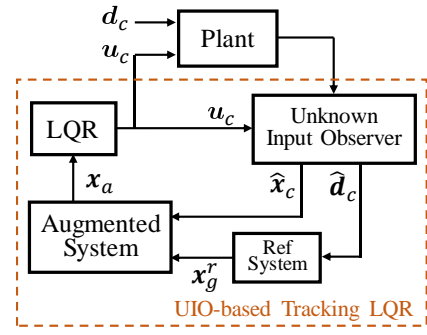


Fig. 6. Architecture and components of the UIO-based tracking LQR

B. The UIO-based Tracking LQR

As noted earlier, the control objective is to let the system frequency track that of a reference system under the same load disturbance. Since this is essentially a tracking problem, we can adopt the LQR to minimize the tracking error. However, to obtain the proper tracking reference in this case, the load disturbance must be estimated. To address this difficulty, the adopted method uses a UIO, and the resulting control architecture is shown in Fig. 6, which also contains a reference system, an augmented system, and an LQR.

The UIO can effectively estimate the system states with the presence of unknown disturbances. Moreover, the disturbance can also be estimated from UIO with the input and output information [30], [31]. The estimated disturbance, $\hat{\mathbf{d}}_c$, is sent to a reference system to generate tracking reference. The reference system represents a “desired version” of the transmission system with desired inertia and droop constants. Therefore, by following the frequency of this reference system, the close-loop system frequency response can be improved to the desired level. The augmented system is simply the combination of the estimated plant states $\hat{\mathbf{x}}_c$, tracking error, and its integral. Then, a standard LQR can be designed based on this augmented system to minimize and eventually eliminate the tracking error. Further details about the design can be found in [18].

C. Control Signal Inversion

Note that, the controller is designed for the combined system. Hence, the control signals should also correspond to the inputs (\mathbf{u}_c) of the combined system model. From (30), \mathbf{u}_c is actually \mathbf{u}_{PV} which comprises two inputs: $\Delta P_{PV}^{ref,a}$ and $\Delta V_{dc}^{ref,a}$, where $\Delta P_{PV}^{ref,a}$ is to be converted to ΔV_{PV}^a by the LUT function g^{-1} . So eventually, the control signals \mathbf{u}_c are mapped to aggregate inputs ($\mathbf{u}^a = [\Delta V_{PV}^a \ \Delta V_{dc}^{ref,a}]^T$) in the aggregate model. However, for practical implementation, we need to obtain the individual control input ($\mathbf{u}_i = [\Delta V_{PV,i} \ \Delta V_{dc,i}^{ref}]^T$) for each of the distributed PV.

Unfortunately, there is no unique way of inverting \mathbf{u}^a back to \mathbf{u}_i . In principle, any inversion would work, as long as satisfying the one-way mapping from \mathbf{u}_i to \mathbf{u}^a , defined in Section II.B. Since the individual control input (\mathbf{u}_i) determines how much PV system’s power output will change, a good strategy is to have the PV systems with higher capability (rated power or irradiance) to contribute with more power. Therefore, adopting this objective, we propose the following inversion rule:

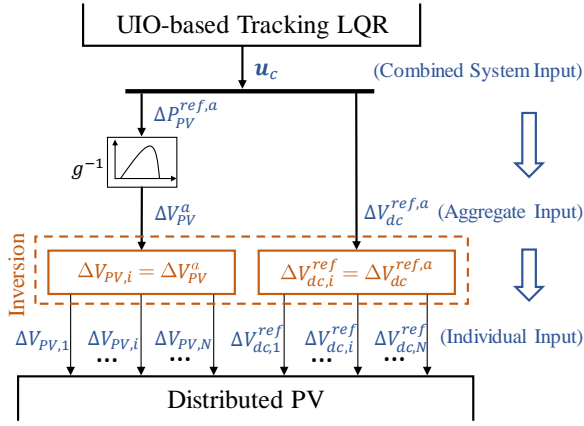
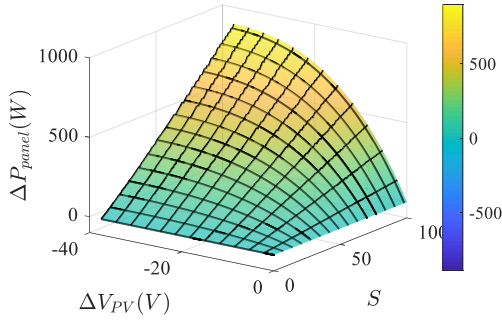


Fig. 7. Inversion of control signals

Fig. 8. The LUT surface of $g(\Delta V_{PV}, S, t)$ for a 5695 W PV panel at 26.85 °C

$$\Delta V_{PV,i} = \Delta V_{PV}^a, \quad \Delta V_{dc,i}^{ref} = \Delta V_{dc}^{ref,a} \quad (32)$$

which corresponds to setting all the individual inputs equal to the aggregate input. This inversion is also illustrated in Fig. 7. First, we can easily verify that this rule meets the mapping from \mathbf{u}_i to \mathbf{u}^a . Then, we will show that this simple, easy-to-implement method is yet very effective to achieve the objective.

c.1) $\Delta V_{PV,i}$: $\Delta V_{PV,i}$ determines the new operating point and thus the steady-state power output of the PV system. Since PV systems consist of identical PV panels connected in parallel (as shown in Fig. 2), the same $\Delta V_{PV,i}$ will result in $\Delta P_{PV,i}$ that are in proportion to the number of PV panels, or equivalently, the rated power.

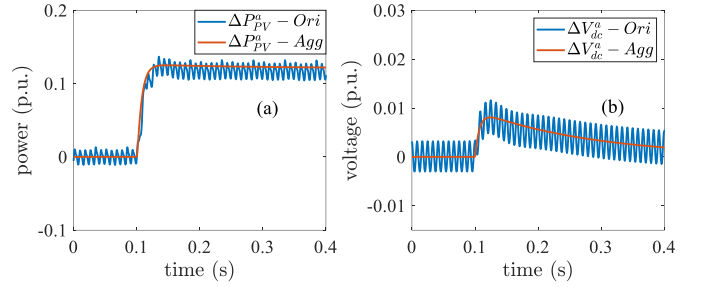
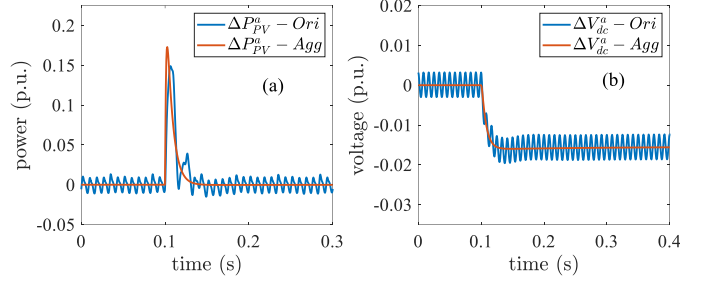
Solar irradiance S is the other main variable that effects the power support capability of a PV system. The LUT surface plotted in Fig. 8 describes the relationship among ΔP_{panel} , ΔV_{PV} , and S . We can easily observe that, for the same value of ΔV_{PV} , the ΔP_{panel} increases as the S becomes higher. Therefore,

TABLE II
DISTRIBUTED PV PARAMETERS WITH VARIATIONS

S_i	[100, 70, 65, 80, 85, 90, 92, 75, 83, 90]
$P_{r,i}$ (KW)	[200, 250, 220, 175, 200, 200, 250, 220, 175, 190]
$k_{p,i}$	[10 15 20 20 17 10 15 20 20 17]
$k_{f,i}$	[50 100 150 80 50 50 100 150 80 50]

TABLE III
INDIVIDUAL AND AGGREGATE CONTROL INPUTS FOR VALIDATION TEST

Individual Input	$\Delta V_{PV,i}$	[-10, -12, -15, -11, -8, -5, -18, -20, -17, -10]
	$\Delta V_{dc,i}^{ref}$	[-10, -5, -8, -7, -5, -4, -9, -11, -6, -12]
Aggregate Input	ΔV_{PV}^a	-12.775 V
	$\Delta V_{dc}^{ref,a}$	-7.730 V

Fig. 9. When $\Delta V_{PV}^a = -12.775$ V, (a) comparison of total increment power ΔP_{PV}^a ; (b) comparison of aggregate DC-link voltage ΔV_{dc}^a Fig. 10. When $\Delta V_{dc}^{ref,a} = -7.730$ V, (a) comparison of total increment power ΔP_{PV}^a ; (b) comparison of aggregate DC-link voltage ΔV_{dc}^a

with the same $\Delta V_{PV,i}$, PV systems under higher S will have more power change in each of their PV panel and thus in the total output as well.

c.2) $\Delta V_{dc,i}^{ref}$: The other control input $\Delta V_{dc,i}^{ref}$ adjusts the DC-link voltage to obtain power from the capacitor. According to (2), this power is proportionally related to the capacitance. We also know that the capacitance should be chosen in proportion to the PV system rated power. Therefore, with the same $\Delta V_{dc,i}^{ref}$, the PV system with larger capacity, and thus capacitance, will have more power released, or absorbed, from its DC-link capacitor.

IV. TEST RESULTS

In this section, we first validate that the reduced-order aggregate model can effectively represent the dynamics of a group of distributed PV. Then, we demonstrate that the UIO-based tracking LQR, which is designed based on the aggregate model, provides effective frequency support during a frequency event. Moreover, we also illustrate the effectiveness of proposed inversion method.

A. Reduced-order Aggregate Model Validation

To validate the proposed reduced-order aggregate model, we first built an IEEE 34 node test feeder in MATLAB/Simulink to represent an area of distribution system. Then, 10 single-phase PV systems are connected to different locations. Each PV system is as illustrated in Fig. 2. We use this test feeder as the benchmark system and compare its overall dynamics with that from the aggregate model. To represent the diversity of distributed PV systems, we choose different values for the solar irradiance, capacity, and control parameters, as listed in TABLE II. For the other basic parameters, we assume them to be the same for every PV system and use the values from Appendix B.

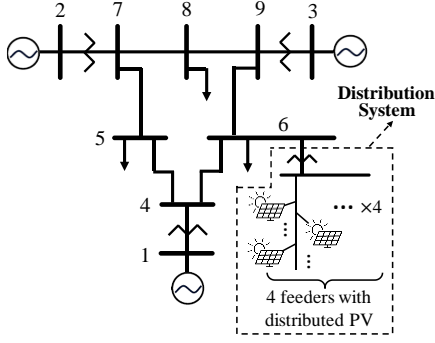


Fig. 11. Modified WECC 9-bus system with distributed PV

TABLE IV
INERTIA AND DROOP USED IN CONTROL DESIGN

	Test System		Reference System	
Inertia	H_g	5.9746 s	H^{ref}	6.2365 s
Droop	R_g	8%	R^{ref}	7.66%

Since the aggregate model is primarily derived for designing frequency support control functions, we are particularly interested in the two relevant quantities: total PV system output power (ΔP_{PV}^a) and aggregate DC-link voltage ($\Delta V_{dc}^{ref,a}$), following the changes in the control inputs. To test, the distributed PV are set to be operating at 85% of their MPPs (nominal de-loading condition). In the first test case, at $t = 1.5$ s, we decrease the PV array voltages by different values as listed in TABLE III. In this case, we expect that the distributed PV to output more power, as all the $\Delta V_{PV,i}$ are negative. For comparison, we calculate the corresponding aggregate control input (ΔV_{PV}^a) and apply it to the aggregate model. We then compare the response of the aggregate model with the calculated aggregate response from the distributed PV in the benchmark system. The comparison results are provided in Fig. 9. In Fig. 9 (a), the total increment power from the aggregate model provides very good approximation to that obtained from the distributed PV. There is slight difference in the steady-state value which is caused by the LUT approximation we made in b.1). Fig. 9 (b) verifies that the aggregate DC-link voltage profile obtained from the aggregate model is very close to that of the distributed PV in benchmark system.

In the second test case, we perturb the other control input which is $\Delta V_{dc,i}^{ref}$. To extract power from DC-link capacitors, we decrease their voltage references by different values as listed in TABLE III. In Fig. 10 (a), fast aggregate power release is observed, and shortly after that, the power decreases to zero as the aggregate DC-link voltage shown in Fig. 10 (b) settles to its steady-state. Fig. 10 (a) and (b) show that the voltage and power profiles from the aggregate model are again very close to those from the distributed PV in benchmark system.

B. Control Performance

To demonstrate the effectiveness of proposed control scheme, we consider the standard three-machine-nine-bus WECC system but modify its capacity down to 116 MVA (S_b) to represent a small-scale power system. Appendix C includes some key parameters of this test system. Then we add four of the IEEE 34 node test feeders at bus 6, as shown in Fig. 11, with each feeder having 10 distributed PV. So, in this test system,

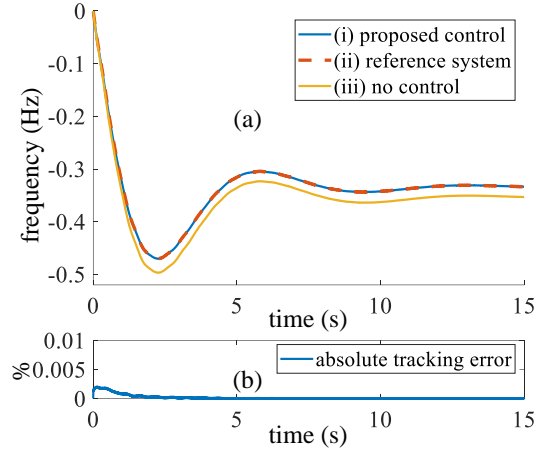


Fig. 12. (a) Frequency response comparison under load disturbance; (b) Absolute error between frequencies of (i) and (ii)

we have 40 distributed PV, and their total capacity is 8.189 MW. Basic parameters of distributed PV are still as summarized in Appendix B, and parameters with diversities are given in Appendix D. The test system is built in MATLAB/Simulink where we conduct time-domain simulations with 5 μ s time resolution for the following study.

To design the UIO-based tracking LQR, we follow the design steps in [18]. The same design parameters are chosen, except for H^{ref} and R^{ref} of the reference system as they should be related to the PV penetration level. In this case, the calculated inertia and droop constants for reference system are provided in TABLE IV, along with those for the original test system without proposed control.

For the test case, we apply a large load disturbance of 0.086 pu at bus 8. Fig. 12 (a) compares the frequency responses obtained from (i) system with proposed control scheme; (ii) reference system; and (iii) system with no frequency support control from distributed PV. From the figure we can clearly see that the frequency with proposed control effectively tracks that of the reference system frequency. The figure also indicates that, by closely following the reference system frequency, the frequency response of the system is improved as desired, specifically in terms of nadir, RoCoF, and settling frequency, compared to that of the original system without control. In Fig. 12 (a), the absolute tracking error between frequencies from (i) and (ii) is also given. We can see that the error is very small with the maximum value being still less than 0.005%.

Next, we want to verify that the proposed inversion method can achieve its design objective. In order to do this, we first select 4 distributed PV systems from the above simulation with the same rated power but different solar irradiance, and plot their power responses in Fig. 13 (a). Per the control signal inversion in (32), they all share the same control inputs. But as shown in the plot, the PV system with higher solar irradiance generate more power as expected, under the same event. In the second case, we choose another set of 4 PV systems with the same irradiance but different rated power. Again, we can see from Fig. 13 (c) that the increment power output are positively correlated to the PV system capacities. In addition, as indicated in Fig. 13 (b) and (d), both of the positive correlations between steady-state ΔP_{PV} and solar irradiance S , ΔP_{PV} and rated power, are almost linear.

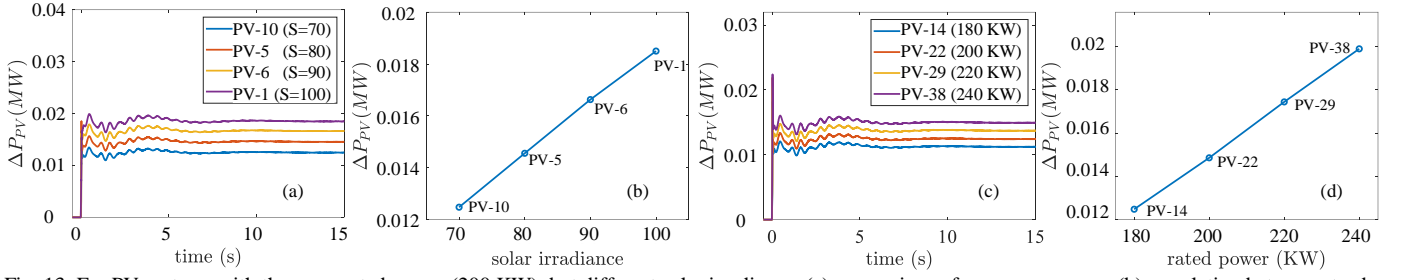


Fig. 13. For PV systems with the same rated power (200 KW), but different solar irradiance: (a) comparison of power responses; (b) correlation between steady-state ΔP_{PV} and S . For PV systems with the same solar irradiance ($S=70$), but different rated power: (c) comparison of power responses; (d) correlation between steady-state ΔP_{PV} and rated power.

V. CONCLUSION

This paper focuses on utilizing distributed PV to provide primary frequency support to the bulk system. For this purpose, we first propose a reduced-order aggregate model to represent the overall dynamic behaviors of a diverse group of distributed PV with varying capacities, solar irradiance, and control parameters. The derived model preserves the same structure and order as that of one PV system. Moreover, inputs needed for the supervisory control are also preserved in the aggregate model. These features greatly facilitate the design of frequency support control. Test results show that the model provides a very close approximation of the response, even under quite large diversity among the distributed PV systems.

This paper also shows that an UIO-based tracking LQR method can be tailored for a group of distributed PV to achieve supervisory frequency support control. An inversion method is also proposed to obtain individual control input for each distributed PV from the aggregate control signal. Simulation results on the test system confirm the effectiveness of both frequency tracking and improvement of the test system frequency response. It is also demonstrated that the proposed inversion method provides an effective way to allocate the total control effort to individual PV systems.

These results also indicate that the proposed control scheme can indeed be adopted by distribution system operators or aggregators for providing frequency support service from distributed PV, especially to small-scale systems with high penetration of distributed PV.

APPENDIX A

$$\begin{cases} \mathbf{A}_{PV} = \begin{bmatrix} 0 & -\frac{1}{C_d P_r^a V_{dc,0}^{ref}} & 0 \\ -\frac{c_P P_r^a V_{sd}}{2\tau} & -\frac{1}{\tau} & \frac{V_{sd}}{2\tau} \\ -c_I P_r^a & 0 & 0 \end{bmatrix} \\ \mathbf{B}_{PV} = \begin{bmatrix} 1 \\ \frac{1}{C_d P_r^a V_{dc,0}^{ref}} \\ 0 \\ 0 \end{bmatrix} \\ \mathbf{C}_{PV} = [0 \quad 1 \quad 0] \end{cases}$$

$$\begin{cases} \mathbf{A}_g = \begin{bmatrix} -\frac{1}{T_g} & 0 & -\frac{1}{R_g T_g} \\ \frac{1}{T_t} & -\frac{1}{T_t} & 0 \\ 0 & \frac{1}{2H_g} & -\frac{D}{2H_g} \end{bmatrix} \\ \mathbf{B}_g = \begin{bmatrix} 0 \\ 0 \\ 1 \\ \frac{1}{2H_g} \end{bmatrix} \\ \mathbf{C}_g = [0 \quad 0 \quad 1] \\ \mathbf{E}_g = \begin{bmatrix} 0 & 0 & -\frac{1}{2H_g} \end{bmatrix}^T \end{cases}$$

APPENDIX B

TABLE V
DISTRIBUTED PV BASIC PARAMETERS

Basic Parameters		
t	Environment temperature	300 K
n_s	# of PV cells per string	500
n_p	# of PV strings	70
C_d	Unit DC-link capacitance	2×10^{-7} F
R	Filter resistance	0.001 Ω
L	Filter inductance	2e-5 H
V_{sd}	Nominal system voltage in d-axis	317 V
$V_{dc,0}^{ref}$	Nominal DC-link voltage	500 V
τ	Current loop time constant	0.001
k_P^i	Current loop control parameter	0.02
k_I^i	Current loop control parameter	1

APPENDIX C

TABLE VI
TEST SYSTEM PARAMETERS

Generators			
	Gen 1	Gen 2	Gen 3
Capacity	50 MVA	41 MVA	25 MVA
Inertia constant	9.55 s	3.33 s	2.35 s
Droop constant	8%	8%	8%
Governor time constant	0.3 s	0.3 s	0.3 s
Turbine time constant	0.8 s	0.8 s	0.8 s
System			
S_b	System Base	116 MVA	
$P_{L,tot}$	Total load	58 MW	
H_g	Equivalent inertia	5.9746 s	
R_g	Equivalent droop	8%	
Distributed PV			
P_r^a	Rated power	8.189 MW	

APPENDIX D

TABLE VII

DISTRIBUTED PV PARAMETERS WITH VARIATIONS IN THE 9-BUS SYSTEM

Parameter	Feeder #	Value
S_i	1	[100, 90, 65, 85, 80, 90, 92, 75, 83, 70]
	2	[95, 85, 90, 70, 77, 75, 88, 83, 96, 100]
	3	[60, 70, 80, 75, 86, 95, 98, 68, 70, 83]
	4	[80, 80, 85, 86, 87, 95, 89, 70, 73, 65]
$P_{r,i}$ (KW)	1	[200, 250, 220, 175, 200, 200, 250, 220, 175, 200]
	2	[250, 220, 230, 180, 190, 220, 200, 240, 190, 195]
	3	[165, 200, 185, 200, 195, 200, 210, 200, 220, 190]
	4	[195, 190, 178, 196, 220, 210, 190, 240, 170, 250]
$k_{p,i}$	1	[10, 15, 20, 20, 17, 10, 15, 20, 20, 17]
	2	[20, 20, 17, 15, 20, 22, 25, 15, 10, 12]
	3	[10, 25, 25, 22, 19, 15, 10, 12, 17, 20]
	4	[17, 19, 16, 20, 25, 23, 22, 20, 20, 17]
$k_{l,i}$	1	[50, 100, 150, 80, 50, 50, 100, 150, 80, 50]
	2	[100, 100, 120, 200, 150, 150, 100, 50, 80, 200]
	3	[50, 80, 80, 95, 120, 110, 100, 100, 80, 75]
	4	[75, 75, 90, 150, 180, 200, 200, 220, 150, 100]

REFERENCES

- [1] U.S. Energy Information Administration, "Annual Energy Outlook 2018," 2018. <https://www.eia.gov/outlooks/aeo/pdf/AEO2018.pdf>.
- [2] National Renewable Energy Laboratory and U.S. Department of Energy, "SunShot Vision Study," 2017. <https://www1.eere.energy.gov/solar/pdfs/47927.pdf>.
- [3] B. Palmintier, R. Broderick, B. Mather, M. Coddington, K. Baker, F. Ding, M. Reno, M. Lave and A. Bharatkumar, "On the path to SunShot. Emerging issues and challenges in integrating solar with the distribution system," National Renewable Energy Lab.(NREL), Golden, CO (United States), 2016.
- [4] G. Barbose, N. Darghouth, D. Millstein, S. Cates, N. DiSanti and R. Widiss, "Tracking the Sun IX: The installed price of residential and non-residential photovoltaic systems in the United States," Lawrence Berkeley National Lab.(LBNL), Berkeley, CA (United States), 2016.
- [5] N.W. Miller, M. Shao, S. Pajic and R. D'Aquila, "Eastern frequency response study," National Renewable Energy Lab.(NREL), Golden, CO (United States), 2013.
- [6] Q. Li and S. Abhyankar, "Evaluation of High Solar Penetration Impact on Bulk System Stability through a Transmission-Distribution Dynamics Co-simulation," In *2019 IEEE Power and Energy Society General Meeting (PESGM)*, 2019.
- [7] Y. Liu, S. You, J. Tan, Y. Zhang and Y. Liu, "Frequency Response Assessment and Enhancement of the US Power Grids Toward Extra-High Photovoltaic Generation Penetrations—An Industry Perspective," *IEEE Trans. Power Syst.*, vol. 33, no.3, pp. 3438-3449, 2018.
- [8] Hydro Quebec, "Transmission Provider Technical Requirements for the Connection of Power Plants to the Hydro Quebec Transmission System," http://www.hydroquebec.com/transenergie/fr/commerce/pdf/exigence_raccordement_fev_09_en.pdf.
- [9] FERC, "Essential Reliability Services and the Evolving Bulk-Power System—Primary Frequency Response" Feb 15, 2018.
- [10] E.N. Code, "Requirements for grid connection applicable to all generators," ENTSO-E: Brussels, Belgium, 2013.
- [11] ERCOT, "Critical Inertia System Operating Limit," http://www.ercot.com/content/wcm/lists/144927/Inertia_Basic_Concepts_Impacts_On_ERCOT_v0.pdf.
- [12] C. Roselund, "Hawaii utilities seek more renewables, storage and now grid services too," *PV Magazine*, "Apr 9," 2019.
- [13] W.A. Omran, M. Kazerani and M. Salama, "Investigation of methods for reduction of power fluctuations generated from large grid-connected photovoltaic systems," *IEEE Trans. Energy Convers.*, vol. 26, no.1, pp. 318-327, 2011.
- [14] H. Xin, Y. Liu, Z. Wang, D. Gan and T. Yang, "A new frequency regulation strategy for photovoltaic systems without energy storage," *IEEE Trans. Sustain. Energy*, vol. 4, no.4, pp. 985-993, 2013.
- [15] A.F. Hoke, M. Shirazi, S. Chakraborty, E. Muljadi and D. Maksimovic, "Rapid Active Power Control of Photovoltaic Systems for Grid Frequency Support," *IEEE Journal of Emerging and Selected Topics in Power Electronics*, vol. 5, no.3, pp. 1154-1163, Sep. 2017.
- [16] W. Im, C. Wang, W. Liu, L. Liu and J. Kim, "Distributed virtual inertia based control of multiple photovoltaic systems in autonomous microgrid," *IEEE/CAA Journal of Automatica Sinica*, vol. 4, no.3, pp. 512-519, 2017.
- [17] X. Lyu, Z. Xu, J. Zhao and K. P. Wong, "Advanced frequency support strategy of photovoltaic system considering changing working conditions," *IET Generation, Transmission & Distribution*, vol. 12, pp. 363-370, 2018.ID: 1.
- [18] Q. Li and M. E. Baran, "A Novel Frequency Support Control Method for PV Plants using Tracking LQR," *IEEE Trans. Sustain. Energy*, pp. 1, 2019.ID: 1.
- [19] M. Datta and T. Senjyu, "Fuzzy Control of Distributed PV Inverters/Energy Storage Systems/Electric Vehicles for Frequency Regulation in a Large Power System," *IEEE Trans. Smart Grid*, vol. 4, pp. 479-488, 2013.ID: 1.
- [20] D. Remon, A.M. Cantarellas, J.D. Nieto, W. Zhang and P. Rodriguez, "Aggregated model of a distributed PV plant using the synchronous power controller," *2015 IEEE 24th International Symposium on Industrial Electronics (ISIE)*, Buzios, 2015, pp. 654-659.
- [21] J. T. Bi, W. Du and H. F. Wang, "Aggregated dynamic model of grid-connected PV generation farms," *International Conference on Renewable Power Generation (RPG 2015)*, pp. 1-6, 2015.ID: 1.
- [22] P.G. Bueno, J.C. Hernández and F.J. Ruiz-Rodríguez, "Stability assessment for transmission systems with large utility-scale photovoltaic units," *IET Renewable Power Generation*, vol. 10, no.5, pp. 584-597, 2016.
- [23] WECC Renewable Energy Modeling Task Force, "WECC solar plant dynamic modeling guidelines," 2014.
- [24] S. Mishra, D. Pullaguram, S. Achary Buragappu and D. Ramasubramanian, "Single-phase synchronverter for a grid-connected roof top photovoltaic system," *IET Renewable Power Generation*, vol. 10, pp. 1187-1194, 2016.ID: 1.
- [25] A. Yazdani and P.P. Dash, "A Control Methodology and Characterization of Dynamics for a Photovoltaic (PV) System Interfaced With a Distribution Network," *IEEE Trans. Power Del.*, vol. 24, no.3, pp. 1538-1551, Jul. 2009.
- [26] N. Arab, B. Kedjar, A. Javadi and K. Al-Haddad, "A Multifunctional Single-Phase Grid-Integrated Residential Solar PV Systems Based on LQR Control," *IEEE Trans. Industry Applications*, vol. 55, pp. 2099-2109, 2019.ID: 1.
- [27] O. Khan and W. Xiao, "An Efficient Modeling Technique to Simulate and Control Submodule-Integrated PV System for Single-Phase Grid Connection," *IEEE Trans. Sustain. Energy*, vol. 7, pp. 96-107, 2016.ID:1.
- [28] Y. Han, M. Luo, X. Zhao, J. M. Guerrero and L. Xu, "Comparative Performance Evaluation of Orthogonal-Signal-Generators-Based Single-Phase PLL Algorithms—A Survey," *IEEE Trans. Power Electronics*, vol. 31, pp. 3932-3944, 2016.ID: 1.
- [29] B. Hauke, "Basic calculation of a boost converter's power stage," Texas Instruments, Application Report, pp. 1-9, November 2009.
- [30] J. Chen and R.J. Patton, *Robust model-based fault diagnosis for dynamic systems*, Springer Science & Business Media, 2012.
- [31] R.J. Patton, P.M. Frank and R.N. Clarke, *Fault diagnosis in dynamic systems: theory and application*, Prentice-Hall, Inc., 1989.